THE JOURNAL OF PHYSICAL CHEMISTRY C
A JOURNAL OF THE AMERICAN CHEMICAL SOCIETY

pubs.acs.org/JPCC

Article

Optical Characterizations for Broadening Emissions from Doping of the Two-Dimensional Tin−Lead Perovskite Films

Sudhakar Narra, Wei-Chuan Chen, Ashank Seetharaman, I-Hua Tsai, and Eric Wei-Guang Diau*

Cite This: *J. Phys. Chem. C* 2024, 128, 1207−1215

Read Online

ACCESS | Metrics & More | Article Recommendations | Supporting Information

ABSTRACT: In this work, we present the optical properties of two-dimensional (2D) perovskite films of $BA_2Sn_xPb_{(1-x)}I_4$ with x = 0−1. The excitonic absorption peaks of the fabricated perovskite samples were shown to shift to lower energies with increase of the Sn proportions in the films, whereas their emission spectra were shown to display dramatic Stokes shifts and spectral broadening from 600 to 1100 nm when compared with their pristine analogues. Power-dependent PL studies indicate that the emissions in the fabricated 2D perovskite samples arise from the self-trapping of excitons, while the spectral broadening originates from the production of multiple defect states upon doping of small amounts of Sn in the Pb-rich samples. The bandwidths of the emission spectra of the Pb−Sn mixed 2D perovskite samples were larger when the Pb proportion was higher than the Sn proportion, a key indicator for increasing the bandwidth of the white-light emission. TA spectral studies reveal that the nature of trap states plays a prominent role in the spectral broadening of the emission of the Pb-rich perovskite samples.

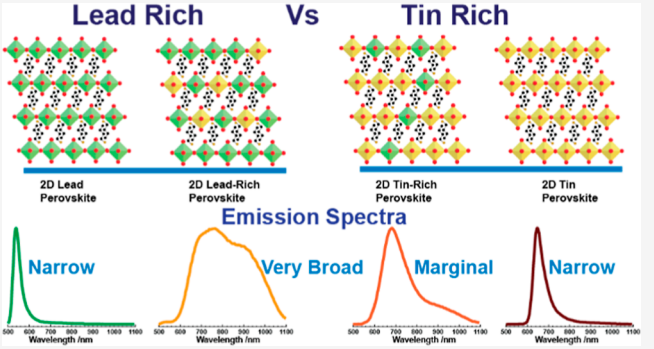

INTRODUCTION

Organic−inorganic hybrid perovskite structures represented by the chemical formula ABX_3 [A is an organic cation, methylammonium (MA^+) or formamidinium (FA^+); B is a metal cation, lead (Pb^{2+}) or tin (Sn^{2+}); X is a halogen anion, chlorine (Cl^-), bromine (Br^-), or iodine (I^-)] have gained tremendous attention due to their simple fabrication procedures with excellent optoelectronic and photovoltaic properties.[1−5] The spatial arrangement of a perovskite is such that monovalent cations (A) are inserted into the BX_6 octahedral holes in a periodic cubic template. However, with a larger size of the bulky organic cation, these octahedral cages can be sliced into layers, generating a nanosheet-like structure. The former relates to a three-dimensional (3D) structure, whereas the latter refers to a two-dimensional (2D) or quasi-2D structure. Ruddlesden−Popper (RP-type) is the most commonly studied quasi-2D structure, expressed as $L_2A_{(n-1)}BX_{3n+1}$, where L is the bulky organic cation to separate the 3D perovskite structure into a quasi-2D layer with $n \geq 1$. In comparison to 3D, the 2D perovskite structure is more stable and exhibits a quantum confinement effect with high exciton binding energy due to the spacer cation L that separates the octahedral layers to form a quantum well structure.[6−8] As a result, photogenerated electron−hole pairs are tightly confined within the octahedral layers, radiatively recombine with high quantum yields, and thereby serve as an excellent candidate for lighting applications.[2,3,9] However, they are still far from commercial development, as obtaining high color purity and efficient LED performance poses a significant challenge.

Various structural engineering techniques, such as implementing a series of spacer cations of bulky organic types, modulating exciton binding energy with different n values, and halide engineering, have been used to tune the emission wavelength from blue to near-infrared (NIR) region and to improve the device performance with external quantum efficiency exceeding 20%.[10−20] Despite these developments, they are constrained by the narrow emission profile with a full width at half-maximum (fwhm) of <50 nm. A broad emission profile with fwhm >100 nm provides selectivity with appropriate band-pass filters and is more suitable for commercial use of lighting applications. To achieve this, a conventional 2D structure can be tweaked to have strong electron−phonon and exciton−phonon couplings as a result of strong lattice distortions, causing excitons or carriers to be self-trapped in the defect states (referred as self-trapped states), resulting in broader emission spectra via self-trap excitons.[20,21] A strong lattice distortion is often achieved by manipulating

Received: November 23, 2023
Revised: December 22, 2023
Accepted: December 28, 2023
Published: January 11, 2024

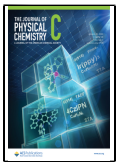

https://doi.org/10.1021/acs.jpcc.3c07717
J. Phys. Chem. C 2024, 128, 1207−1215

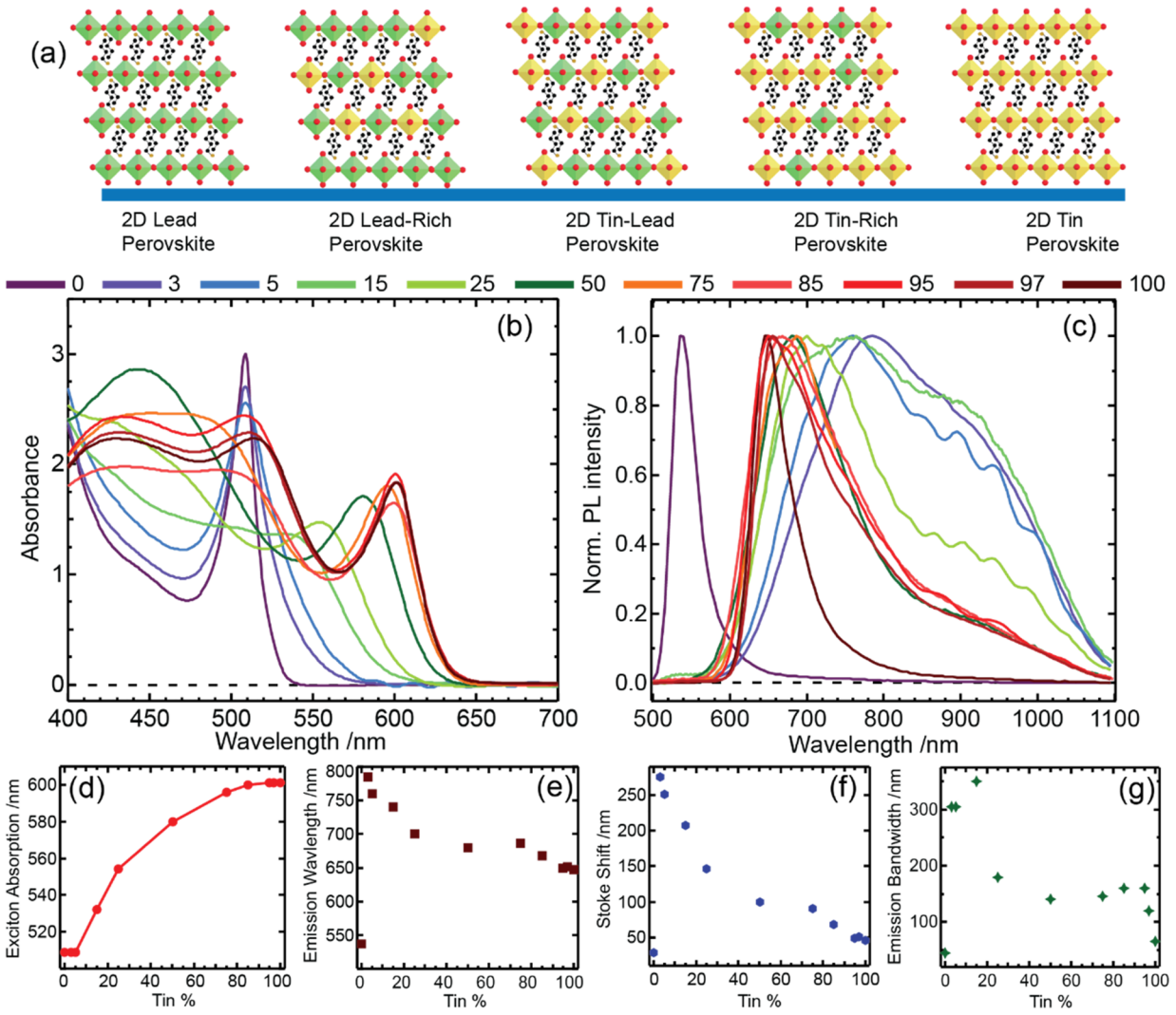

Figure 1. (a) Schematic perovskite structures and (b) UV−vis and (c) PL spectra of the $BA_2Pb_{(1-x)}Sn_xI_4$ samples with $0 < x < 1$. The legends represent the percentage proportions of the Sn^{2+} content in the BA_2PbI_4 films. (d) Excitonic absorption peak maxima, (e) emission peak maxima, (f) Stokes shift between absorption and emission peak maxima, and (g) emission bandwidth of the $BA_2Pb_{(1-x)}Sn_xI_4$ samples are shown. The abscissa is shown in the percentage proportions of tin.

the B−X bond using larger spacer cations, by adjusting the A/L ratio, and through metal doping. The first report on broad emissions in perovskite was demonstrated by introducing larger spacer cations and a mixed halide system.[22] Similarly, various studies on broad and white light emission based on modulation in spacer cations and halide ions have been reported.[23−29] Broader emission was also observed in heterophane α/δ-$CsPbI_3$ without external doping, where a thermal annealing method was used to form an additional phase.[30] This phase induced self-trapped states, allowing charges to be injected into the parent phase. Furthermore, broad emission due to Sn doping provided an alternating approach in 2D Pb perovskites.[31−35] The spectral broadening in mixed 2D Sn−Pb perovskites has been attributed to Sn vacancies,[32] charge transfer excitons,[33] defects,[34] and self-trapped excitons,[31,35] making the underlying mechanism complicated. However, there is no clear picture on the distribution of Sn or Pb dopants in the bulk of the 2D structure under lead-rich, tin-rich, and mixed Sn−Pb conditions. Hence, a correlation between the defect nature and emission spectral broadening is yet to be fully understood.

Here, in this report, we fabricated thin films of 2D ($n = 1$) tin−lead perovskites with butylammonium (BA) as the spacer cations, formulated as $BA_2Sn_xPb_{(1-x)}I_4$, ($x = 0-1$). Broad emissions covering the spectral range of 600−1100 nm were observed for the lead-rich perovskite samples. The photophysical characterizations were performed using UV−vis absorption, photoluminescence (PL), time-correlated single photon counting (TCSPC), and femtosecond transient absorption spectroscopy (TAS) techniques. TAS studies showed that the defect centers play an important role in accounting for the spectral broadening emissions of the 2D perovskites.

METHODS

The 2D perovskite thin film samples were cast from their respective precursor solutions onto a high cleaned, dried, and ozonized circular glass substrate using the spin-coating technique inside a glovebox which was maintained at the steady flow of nitrogen during fabrication. The diameter and thickness of the glass substrate used are 25.4 and 1 mm, respectively. The glass substrates were pretreated with UV light

https://doi.org/10.1021/acs.jpcc.3c07717
J. Phys. Chem. C 2024, 128, 1207−1215

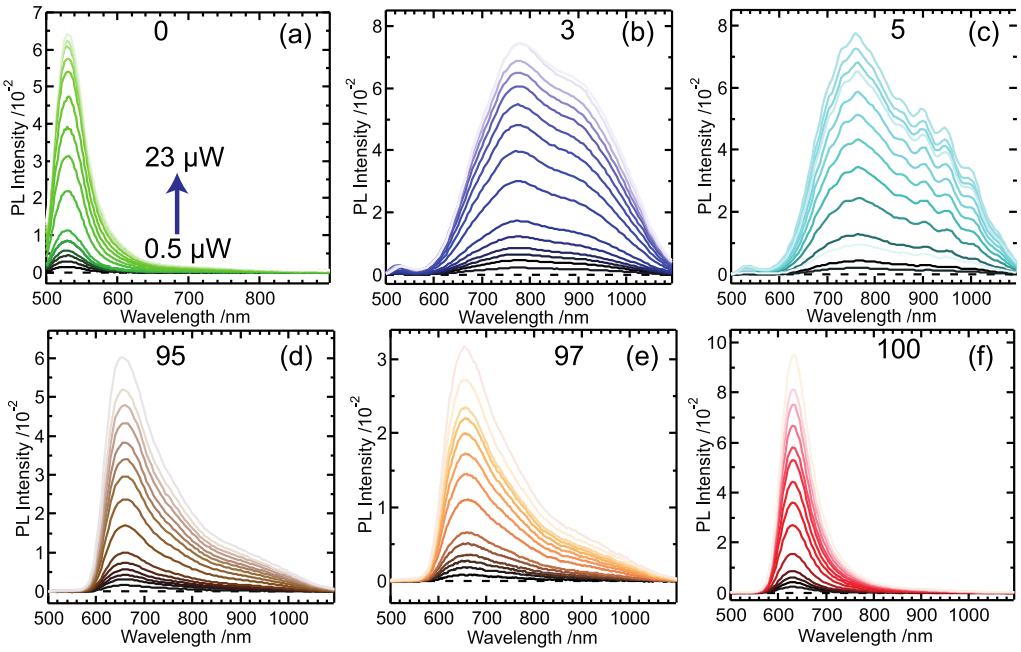

Figure 2. Fluence-dependent PL spectra of $BA_2Pb_{(1-x)}Sn_xI_4$ films, where x = (a) 0, (b) 0.03, (c) 0.05, (d) 0.95, (e) 0.97, and (f) 1, respectively.

and ozone for 30 min prior to spin-coating after completion of cleaning and drying procedures. The glovebox is maintained at minimal levels of oxygen and water vapor to ensure no sample degradation during fabrication as indicated, i.e., $O_2 \leq 2$ ppm and $H_2O \leq 0.5$ ppm. 0.8 M concentrated precursor solutions of BA_2PbI_4 and BA_2SnI_4 in DMF were prepared and were intermixed appropriately to generate $BA_2Pb_{(1-x)}Sn_xI_4$ precursor solutions with compositions of x varying from 0 (0%), 0.03 (3%), 0.05 (5%), 0.15 (15%), 0.25 (25%), 0.5 (50%), 0.75 (75%), 0.85 (85%), 0.95 (95%), 0.97 (97%), and 1 (100%). The percentages represent the percentage of Sn^{2+} ions in the films. The corresponding precursor solutions were spread uniformly onto glass substrates loaded on the spin coater rotor, and the substrates were spun at a rate of 8000 rpm for 56 s. Later, the films were annealed at 70 °C for 10 min on a hot plate inside the glovebox. Furthermore, the fabricated 2D perovskite films were packaged inside the glovebox itself by encapsulating them with another bigger glass substrate (diameter 36 mm) where the edges of both the substrates are bonded together using UV glue (Norland 61, Thorlabs NOA61). This method ensures the stability of the perovskites from degradation due to ambient O_2 and water vapor. The low dimensional phases of the fabricated 2D perovskites were confirmed by measuring the XRD spectra of the respective samples (unencapsulated), as shown in Figure S1, using an X-ray diffractometer (Bruker D8). The samples were transported in airtight nitrogen flushed bags to the measurement facility and the measurement time or exposure time of samples to air is about 6 min.

A Jasco-V-780 UV−visible/NIR spectrophotometer equipped with an integration sphere accessory (ISN-9011, Jasco) was used to measure the absorption spectra of the fabricated 2D perovskite thin-film samples. The absorption spectra are measured in the range of 350−900 nm with a spectral resolution of 1 nm and scan speed of 400 nm/min. The absorption spectra were corrected for reflection and substrate losses. The PL spectra of 2D perovskite samples were measured from a laboratory-built PL system as described. Briefly, we excited the samples using 450 nm excitation light obtained from a CW diode laser (MDL-III-450−100 mW; power supply: PSU-III-FDA) and the emission spectrum was measured by scanning the grating of the monochromator (Dongwoo, DM150i, blaze at 750 nm; groove density 600 gr/mm). The excitation light is cut off using a long pass filter. The dispersed light from the monochromator is focused onto a Si-photodiode detector (TE-cooled, Sciencetech Inc. S-025-TE2-H; power supply PS/TC-1) coupled to a digital multimeter (DMM4020). The PL lifetimes of the 2D perovskite samples were measured using a PicoQuant-FluoTime 200 TCSPC system. 2D perovskite films were excited using a 440 nm picosecond diode laser (LDH-P-C-440, fwhm: 60 ps, controller: PLD 200-B). The PL lifetimes were obtained from the decay traces obtained from the respective PL spectral maxima. The morphology of 2D perovskite samples was examined using a field-emission scanning electron microscope (FESEM, Hitachi SU8010). The samples' exposure to air while loading the samples onto the sample stage of the SEM machine and inserting them into the chamber was less than 2 min.

The femtosecond transient absorption spectra were measured by using an ExciPro ultrafast pump−probe spectrometer utilizing a femtosecond Ti/sapphire amplified laser system (Coherent Legend USP, 795 nm, 1 kHz, 3 mJ, 35 fs) to generate excitation and probe pulses. The excitation is obtained by frequency doubling (397 nm) of the fundamental of the amplifier on a BBO crystal, while the white-light continuum probe pulses were generated using a sapphire plate. The white light is generated by pumping the sapphire plate with fundamental laser pulse for measuring the TAS profiles in the shorter-wavelength region (450−700 nm), while the 1300 nm pulse obtained from the optical parametric amplifier (TOPAS-C) was used to generate the white light for the longer-wavelength region (700−980 nm). The pump and probe pulses were set to magic angle, and the obtained transient spectra were corrected for chirp and denoised using a singular value decomposition algorithm.

https://doi.org/10.1021/acs.jpcc.3c07717
J. Phys. Chem. C 2024, 128, 1207−1215

RESULTS AND DISCUSSION

2D perovskites with the chemical formula $BA_2Sn_xPb_{(1-x)}I_4$, (x = 0−1) (Figure 1a) were fabricated according to the experimental procedures detailed in the Methods section. The XRD patterns shown in Figure S1 confirm the formation of low dimensional phases with intense peaks at 6.4°, corresponding to the (002) orientation.[36,37] Intermixing of Pb with Sn or the other way around produced only a small change in the XRD patterns. The SEM images shown in Figure S2 confirm that layered structures were produced successfully, but a clear distinction between the Pb-rich and Sn-rich samples was observed for the grain sizes and overall film morphologies. The pristine BA_2PbI_4 sample showed smaller grains with a lot of grain edges; in contrast, pristine BA_2SnI_4 displayed larger grains. Furthermore, doping Pb-rich samples with Sn^{2+} ions localized the defects at grain edges at lower concentrations (e.g., 3%) which progressively penetrated into the grain interiors at 25 and 50% concentrations along with the increase of the grain size. However, Sn-rich samples do not offer such a doping effect in the grain edge and interior. The optical properties of the fabricated 2D perovskite samples were characterized using UV−vis absorption and PL spectra as shown in Figure 1b,c, respectively. Both absorption and PL spectra of the 2D perovskite films show a red shift upon incorporating the Sn^{2+} ions into the native Pb^{2+} ion positions of the BA_2PbI_4 film. Apart from the spectral shifts, the absorption spectra (Figure 1b) show weakened and broader excitonic features, whereas the PL spectra (Figure 1c) show large Stokes shifts with asymmetrical broadening of the spectra.

The exciton absorption shows shifts from 510 to 605 nm upon increasing the proportion of Sn^{2+} as shown in Figure 1d, while the PL peak positions shifted from 540 to 800 nm when a smaller proportion of Sn^{2+} doping (3%) was involved (Figure 1e). Furthermore, there seemed to be a correlation between the Stokes shifts and the PL spectral bandwidth within the experimental uncertainties, as shown in Figure 1f,g, respectively. The large Stokes shift and broad PL emission band in the Pb-rich 2D perovskite samples were assigned to emission due to self-trapping of excitons.[29,31] In contrast to the Pb-rich samples, Sn-rich samples show modest broadening and small Stokes shifts, suggesting that the mechanism of spectral broadening between these two cases should come from different origins. Overall, the UV−vis and PL spectral data show that doping of the 2D perovskite films with either Sn^{2+} or Pb^{2+} ions leads to spectral broadening, which is more pronounced in the Pb^{2+} case than in the Sn^{2+} case. The origins of emission broadening can be understood according to the fluence-dependent PL spectra shown in Figures 2 and S3. Furthermore, the fluence-dependent growth of band intensities was fitted to a power law (Figure S4) and the exponents of the power law were plotted against the Sn proportion in Figure S5a. From the exponents, the PL band intensities show sublinear growth with laser fluence for most samples except for the 15%- and 25%-doped samples. The sublinear growth of PL band intensities indicates that the underlying mechanism behind the emission in the 2D perovskites is predominantly due to formation of defects caused by structural distortions or vacancies in the pristine samples and extrinsically doping Sn−Pb samples. The superlinear growth observed for 15 and 25% samples could be due to the change of the defect nature in these samples. The shift of dopant aggregation from the grain edges to grain interiors shown in the SEM images (Figure S2) for these Sn-rich samples validates the aforementioned explanation. The theoretical model on fluence-dependent PL intensities applied to simulating chalcopyrite films suggests that the presence of deep-level defect states can transcend the PL band intensity growth from sublinear to superlinear as we observed herein (Figure S5a).[35,38] The sublinear growth of PL band intensities in both Pb-rich and Sn-rich 2D perovskites with different magnitudes of Stokes shifts and spectral broadening suggests that the nature of defects is drastically different in both cases, which will be further discussed in the later sections.

PL lifetimes of 2D perovskite films were studied using the TCSPC technique as shown in Figure 3. The pristine Pb/Sn

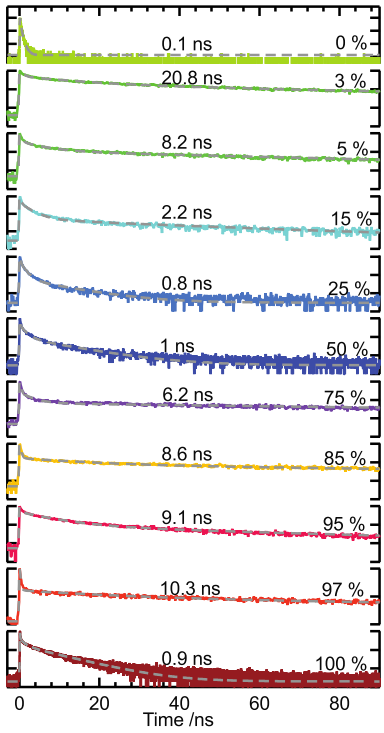

Figure 3. (a) TCSPC decay profiles of the $BA_2Pb_{(1-x)}Sn_xI_4$ samples with $0 < x < 1$. The legends represent the percentage proportions of the Sn^{2+} content in the BA_2PbI_4 films.

samples, BA_2PbI_4 and BA_2SnI_4, showed shorter PL lifetimes when compared to those of the mixed Sn−Pb samples. The lifetimes of the mixed Sn−Pb samples in varied Sn proportions showed a minimal lifetime near 25 to 50% of Sn^{2+} compositions. The decrease of lifetimes for the 25 to 50% samples is due to the surface defects moving from grain boundaries to grain interiors, as shown in the SEM images (Figure S2).

Femtosecond TAS measurements were performed on 2D perovskite films by exciting them using an excitation wavelength of 397 nm and probed in the region of 470−970 nm. The TA spectra were split into two parts to describe the effects of optical excitation on the band-edge and the sub-band gap regions. Figures 4 and 5 show the TAS profiles of 0, 3, 5, 95, 97, and 100% Sn samples, while Figures S6 and S7 show the TAS profiles of 15, 25, 50, 75, and 85% Sn samples for band-edge and sub-band gap probe regions, respectively.

The TAS profiles for the band-edge region shown in Figures 4 and S6 exhibit depletion of excitonic states with a second derivative shape being preserved until the nanosecond time

https://doi.org/10.1021/acs.jpcc.3c07717
J. Phys. Chem. C 2024, 128, 1207−1215

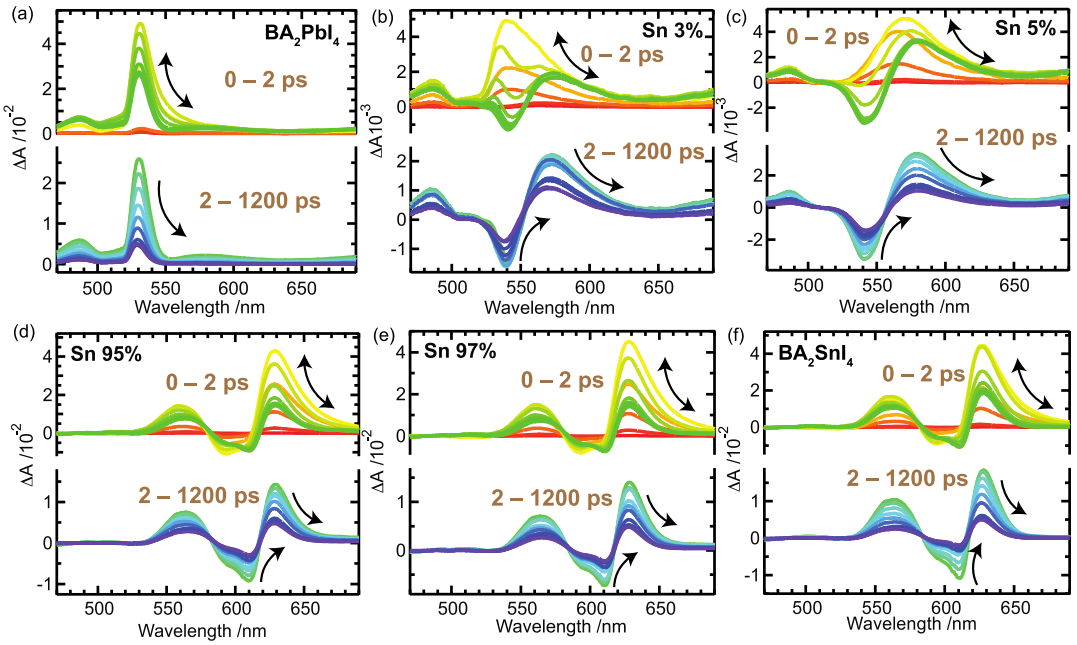

Figure 4. Band-edge TA spectra of (a) 0, (b) 3, (c) 5, (d) 95, (e) 97, and (f) 100% Sn perovskite samples. The top panels show TA spectra between 0 and 2 ps, and the bottom panel shows TA spectra between 2 and 1200 ps as indicated.

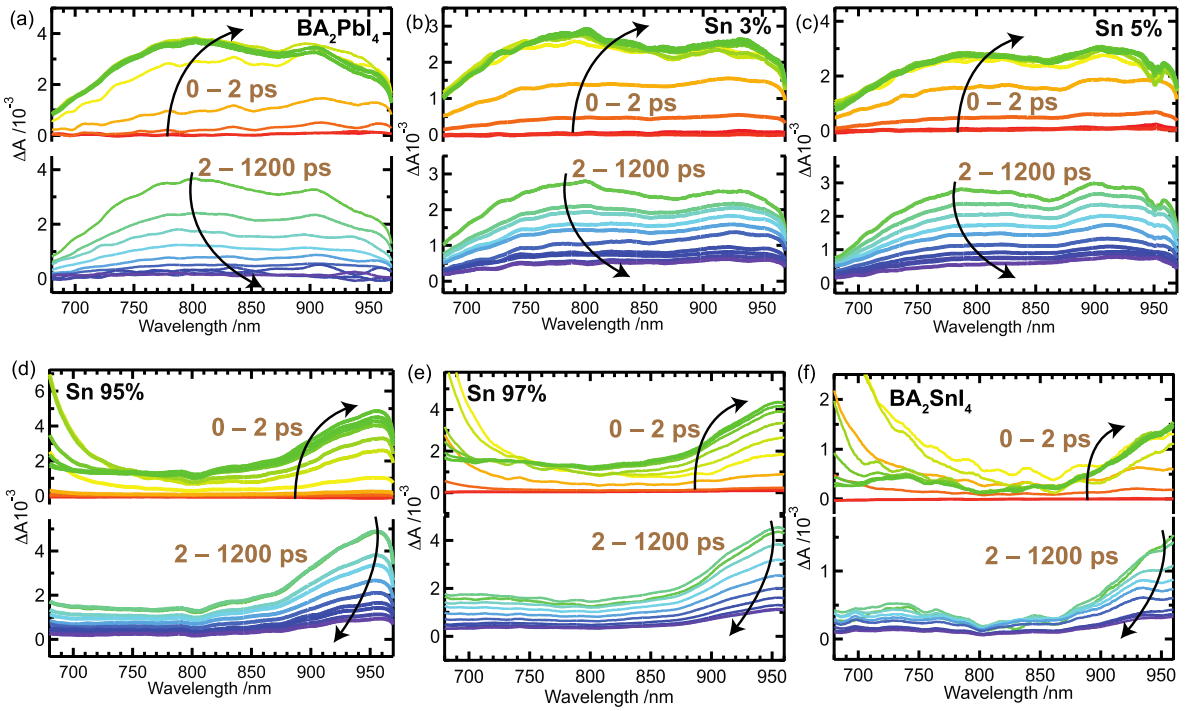

Figure 5. Sub-band gap TA spectra of (a) 0, (b) 3, (c) 5, (d) 95, (e) 97, and (f) 100% Sn perovskite samples. The top panels show TA spectra between 0 and 2 ps and the bottom panel shows TA spectra between 2 and 1200 ps as indicated.

scale region. 0 and 3% Sn samples show weaker or no depletion of the excitonic bands probably due to the overlap of the strong PIA band with the ground state excitonic band. The positions of the exciton depletion band minima show progressive red shifts which are consistent to their ground-state excitonic absorption profiles. The asymmetric second derivative shape of the TAS profiles could be an admix of both band gap renormalization (BGR) and band broadening (BB) of the excitonic states,[39−41] forbidden exciton,[42] or biexciton.[43−45] The recoveries of spectral bands in the range of 2−1200 ps (Figure 4b−f) show isosbestic points indicating that the origin of both depletion and photoinduced absorption should come from similar origin, favoring BB processes as the underlying mechanism showing the TAS profiles on the longer time scales. The PIA bands due to biexcitons were shown to display a lifetime of several tens of picoseconds in lead perovskite quantum wells;[45] however, the PIA bands shown in Figure 4 display much greater lifetimes. On the other hand, the BGR process induces the first derivative shape as it involves shift of band gap, whereas forbidden excitonic levels are shown

https://doi.org/10.1021/acs.jpcc.3c07717
J. Phys. Chem. C 2024, 128, 1207−1215

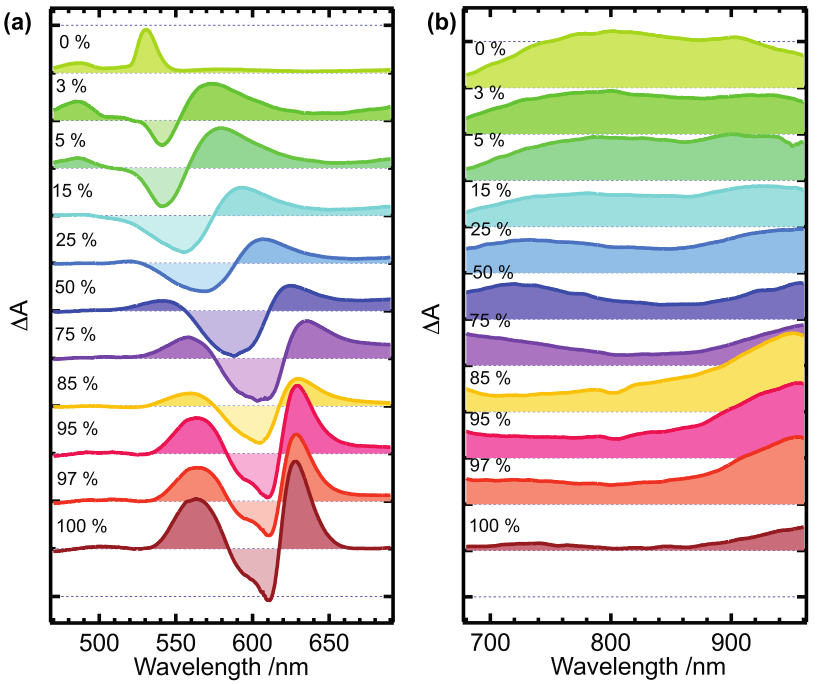

Figure 6. Composition-dependent TAS spectra of Sn−Pb 2D perovskite samples probed in the (a) 470−680 and (b) 680−960 nm regions. The Sn proportions are indicated in the legends.

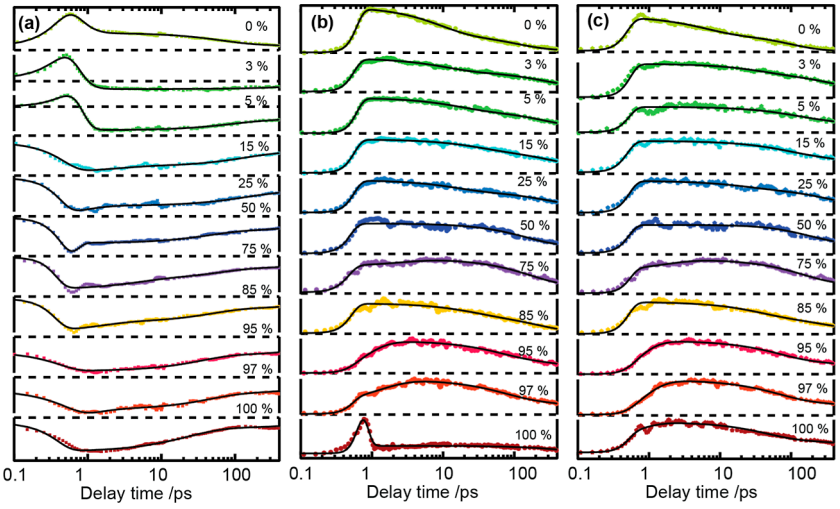

Figure 7. Composition-dependent TAS kinetics of Sn−Pb samples probed at (a) PB band minima (peak position) and (b) 800 and (c) 900 nm regions. The Sn proportions are indicated in the legends. The zero time is offset to show the baseline at a negative time.

as PIA bands on the higher-energy side of the spectra,[42] in contrast to the spectral profiles presented here. Therefore, BB might be the dominant origin of the observed TAS profile shapes on the picosecond time scales, whereas contributions from the other processes aforementioned cannot be ruled out in the subpicosecond region after photoexcitation. Furthermore, the ΔA values for excitonic depletion bands of Pb-rich samples are 1 order of magnitude smaller than the Sn-rich samples due to efficient splitting of excitons to carriers in the latter for their lower excitonic binding energies compared to the former.[46] A similar explanation has been used to account for the efficient splitting of excitons to carriers in the case of Pb perovskite quantum wells.[47] Therefore, the observed BB of the TAS profiles can be attributed to the interaction of excitons with defects at grain boundaries or grain interiors (as shown in the SEM images of Figure S2) due to localization of excitons (or carriers).

The trap-state-mediated absorption profiles were observed by monitoring the TAS profiles of the 2D perovskite films probed in the 700−960 nm region as shown in Figures 5 and S7. Pb-rich 2D perovskite samples with tin of 0, 3, and 5% show broad absorption covering the whole of the probe region, while the Sn-rich samples with tin of 95, 97, and 100% show a downward curvature shape in the trap-state absorption band indicating that the defect centers observed in Pb-rich and Sn-rich samples are of different origins, responsible for different magnitudes of PL spectral broadening. It is interesting to note that both pristine BA_2PbI_4 and BA_2SnI_4 showed defect-state TA bands that are identical to lead-rich (e.g., 3%) and tin-rich (e.g., 97%) samples, respectively. However, the emission

https://doi.org/10.1021/acs.jpcc.3c07717
J. Phys. Chem. C 2024, 128, 1207−1215

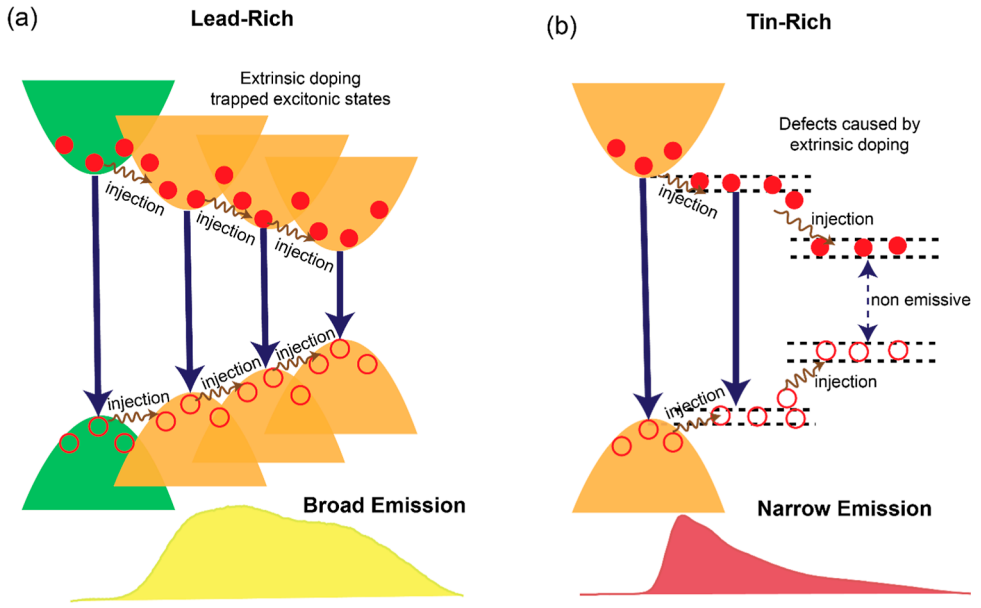

Figure 8. Mechanism to explain the spectral broadening of the emission in (a) lead-rich samples compared to (b) tin-rich samples.

spectra of the pristine samples are much narrower than those of their doping analogues. It implies that additional dopants take over the native sites, creating the acceptor-type defect states that lead to spectral broadening of the emission. Therefore, the TAS profiles presented in Figure 5 serve as a crucial indicator of the mechanism of spectral broadening in these samples.

Furthermore, the TAS profiles of varied compositions were plotted with increments of Sn proportions as shown in Figure 6. Figure 6a shows the band-edge TAS profiles, while Figure 6b shows the sub-band gap profiles with the signatures of the trap states obtained at 2 ps after the excitation. Band-edge TAS profiles (Figure 6a) show that BB effects on Sn-rich samples are greater so that splitting of excitons to carriers is higher in the Sn-rich samples than in the Pb-rich samples, which is consistent with smaller binding energies of the 2D Sn-rich perovskites compared with their Pb-rich counterparts.[46] The TAS profiles in the sub-band gap region (Figure 6b) show that the Pb-rich samples exhibit broad uniform distribution of the PIA bands in the probed region, while Sn-rich samples show PIA bands localizing at the longer-wavelength or lower-energy region, which implies a different defect nature compared to the former case.

The TAS decay profiles of the perovskite films as a function of the Sn proportions are shown in Figure 7. The TAS bands monitored at peak positions of the exciton bands are shown in Figure 7a while the TAS bands monitored on dark trap states at 800 and 900 nm are shown in Figure 7b,c, respectively. All of the transient decay profiles can be fairly fitted with a triple exponential function. The fitting results are presented in Tables S1−S3. The fitted time coefficients are consistent with the trend of the average PL lifetimes. The three decaying processes associated with the band-edge profiles can be assigned to thermalization (τ_1), localized excitons (carriers) at defects (τ_2), and radiative recombination processes (τ_3). For PIA bands at 800 and 900 nm, the time coefficients are much greater when compared to those of the band-edge profiles, suggesting that the recombination pathways of the PIA bands are different from those of the band-edge profiles.

The emission spectral bandwidths of Pb-rich and Sn-rich samples exhibited different results despite structural similarity shown by XRD and a similar defect-based emission mechanism shown by the fluence-dependent PL spectra with exponents of the power law lying mostly under 1. However, TAS profiles probed in the sub-band gap region revealed the distinction between the distribution of the trap-state absorption bands for Pb-rich and Sn-rich samples as shown in Figures 5 and 6. The broad spectral distribution of the trap states in the Pb-rich sample suggests that structural distortions with varied configurations might be involved. In the case of the Sn-rich samples, the trap-state absorption bands with a band maxima at 960 nm might be coming from deep-trap defects along with the shallow-trap defects observed from the band tails at the 700 nm region. For the Pb-rich perovskites, doping with small-band gap Sn perovskites creates an acceptor state that led to emission from the sub-band gap region as illustrated in Figure 8a. The broad emission of the Pb-rich samples can be assigned to self-trapping of excitons as proposed in other reports.[34,35] In contrast, in the case of Sn-rich perovskites, oxidation of Sn leads to Sn vacancies that can lead to both shallow- and deep-trap states.[36] It is shown that Sn vacancies can broaden the emission,[32] but the bandwidth might be narrower compared to the Pb-rich case as the deep-trap states are often nonemissive as indicated in Figure 8b. Therefore, the results presented here suggest that tweaking of the defect states and doping atoms together with favorable dopants are key to producing broader and intense emission spectra in 2D perovskites.

CONCLUSIONS

Two dimensional (2D) perovskite $BA_2Pb_{(1-x)}Sn_xI_4$ films with $0 < x < 1$ fabricated using a one-step solution process showed progressive red shifts in the absorption spectra of the samples with increase in the concentration of Sn contents. The PL spectra of the mixed Sn−Pb perovskite samples were shown to possess large Stokes shifts in the PL band maxima and broader emission spectral widths compared with their respective pristine counterparts. The PL emission bands were shown to be broader for the Pb-rich samples compared to the Sn-rich samples. The TAS profiles of band edges showed splitting of

https://doi.org/10.1021/acs.jpcc.3c07717
J. Phys. Chem. C 2024, 128, 1207−1215

excitons at the grain boundaries with their characteristic second derivative shapes, while the sub-band gap TAS profiles show that the defect centers were quite distinct between the Pb-rich and Sn-rich samples with the former showing uniform trap density absorption in the 700−1000 nm region, whereas the latter displaying distinct trap density absorption near 960 nm. The differences in the PL spectral broadening for Pb-rich and Sn-rich samples were shown to be due to the differences in the mechanisms of emission as the former emitting via self-trapped excitons and the latter emitting via shallow-trap states, as shown in Figure 8.

■ ASSOCIATED CONTENT

Supporting Information

The Supporting Information is available free of charge at https://pubs.acs.org/doi/10.1021/acs.jpcc.3c07717.

XRD patterns, SEM images, TAS profiles, fluence-dependent PL spectra, and curve fitting results (PDF)

■ AUTHOR INFORMATION

Corresponding Author

Eric Wei-Guang Diau − *Department of Applied Chemistry and Institute of Molecular Science, National Yang Ming Chiao Tung University, Hsinchu 300093, Taiwan; Center for Emergent Functional Matter Science, National Yang Ming Chiao Tung University, Hsinchu 300093, Taiwan;* orcid.org/0000-0001-6113-5679; Email: diau@nycu.edu.tw

Authors

Sudhakar Narra − *Department of Applied Chemistry and Institute of Molecular Science, National Yang Ming Chiao Tung University, Hsinchu 300093, Taiwan; Center for Emergent Functional Matter Science, National Yang Ming Chiao Tung University, Hsinchu 300093, Taiwan;* orcid.org/0000-0003-4893-9204

Wei-Chuan Chen − *Department of Applied Chemistry and Institute of Molecular Science, National Yang Ming Chiao Tung University, Hsinchu 300093, Taiwan*

Ashank Seetharaman − *Department of Applied Chemistry and Institute of Molecular Science, National Yang Ming Chiao Tung University, Hsinchu 300093, Taiwan;* orcid.org/0000-0002-4417-8631

I-Hua Tsai − *Department of Applied Chemistry and Institute of Molecular Science, National Yang Ming Chiao Tung University, Hsinchu 300093, Taiwan*

Complete contact information is available at: https://pubs.acs.org/10.1021/acs.jpcc.3c07717

Notes

The authors declare no competing financial interest.

Published as part of *The Journal of Physical Chemistry C* virtual special issue "Hiroaki Misawa Festschrift".

■ ACKNOWLEDGMENTS

This work was supported by the National Science and Technology Council (grant nos. NSTC 111-2634-F-A49-007, NSTC 111-2123-M-A49-001, and NSTC 112-2639-M-A49-001-ASP) and Center for Emergent Functional Matter Science of National Yang Ming Chiao Tung University (NYCU) from The Featured Areas Research Center Program within the framework of the Higher Education Sprout Project by the Taiwan Ministry of Education (MOE).

■ REFERENCES

(1) Park, N.-G. Perovskite Solar Cells: An Emerging Photovoltaic Technology. *Mater. Today* **2015**, *18* (2), 65−72.

(2) Wang, K.; Park, J. Y.; Akriti; Dou, L. Two-Dimensional Halide Perovskite Quantum-Well Emitters: A Critical Review. *EcoMat* **2021**, *3* (3), No. e12104.

(3) Pedesseau, L.; Sapori, D.; Traore, B.; Robles, R.; Fang, H.-H.; Loi, M. A.; Tsai, H.; Nie, W.; Blancon, J.-C.; Neukirch, A.; et al. Advances and Promises of Layered Halide Hybrid Perovskite Semiconductors. *ACS Nano* **2016**, *10* (11), 9776−9786.

(4) Tsai, H.; Nie, W.; Blancon, J.-C.; Stoumpos, C. C.; Asadpour, R.; Harutyunyan, B.; Neukirch, A. J.; Verduzco, R.; Crochet, J. J.; Tretiak, S.; et al. High-Efficiency Two-Dimensional Ruddlesden? Popper Perovskite Solar Cells. *Nature* **2016**, *536* (7616), 312−316.

(5) Sirbu, D.; Balogun, F. H.; Milot, R. L.; Docampo, P. Layered Perovskites in Solar Cells: Structure, Optoelectronic Properties, and Device Design. *Adv. Energy Mater.* **2021**, *11* (24), 2003877.

(6) Li, X.; Hoffman, J. M.; Kanatzidis, M. G. The 2D Halide Perovskite Rulebook: How the Spacer Influences Everything from the Structure to Optoelectronic Device Efficiency. *Chem. Rev.* **2021**, *121* (4), 2230−2291.

(7) Smith, M. D.; Crace, E. J.; Jaffe, A.; Karunadasa, H. I. The Diversity of Layered Halide Perovskites. *Annu. Rev. Mater. Res.* **2018**, *48* (1), 111−136.

(8) Hoye, R. L. Z.; Hidalgo, J.; Jagt, R. A.; Correa-Baena, J.; Fix, T.; MacManus-Driscoll, J. L. The Role of Dimensionality on the Optoelectronic Properties of Oxide and Halide Perovskites, and their Halide Derivatives. *Adv. Energy Mater.* **2021**, *12*, 2100499.

(9) Mao, L.; Stoumpos, C. C.; Kanatzidis, M. G. Two-Dimensional Hybrid Halide Perovskites: Principles and Promises. *J. Am. Chem. Soc.* **2019**, *141* (3), 1171−1190.

(10) Yang, X.; Zhang, X.; Deng, J.; Chu, Z.; Jiang, Q.; Meng, J.; Wang, P.; Zhang, L.; Yin, Z.; You, J. Efficient Green Light-Emitting Diodes Based on Quasi-Two-Dimensional Composition and Phase Engineered Perovskite with Surface Passivation. *Nat. Commun.* **2018**, *9* (1), 570.

(11) Yuan, F.; Zheng, X.; Johnston, A.; Wang, Y.-K.; Zhou, C.; Dong, Y.; Chen, B.; Chen, H.; Fan, J. Z.; Sharma, G.; et al. Color-Pure Red Light-Emitting Diodes Based on Two-Dimensional Lead-Free Perovskites. *Sci. Adv.* **2020**, *6* (42), No. eabb0253.

(12) Jiang, Y.; Qin, C.; Cui, M.; He, T.; Liu, K.; Huang, Y.; Luo, M.; Zhang, L.; Xu, H.; Li, S.; et al. Spectra Stable Blue Perovskite Light-Emitting Diodes. *Nat. Commun.* **2019**, *10* (1), 1868.

(13) Guo, B.; Lai, R.; Jiang, S.; Zhou, L.; Ren, Z.; Lian, Y.; Li, P.; Cao, X.; Xing, S.; Wang, Y.; et al. Ultrastable Near-Infrared Perovskite Light-Emitting Diodes. *Nat. Photonics* **2022**, *16* (9), 637−643.

(14) Jiang, J.; Chu, Z.; Yin, Z.; Li, J.; Yang, Y.; Chen, J.; Wu, J.; You, J.; Zhang, X. Red Perovskite Light-Emitting Diodes with Efficiency Exceeding 25% Realized by Co-Spacer Cations. *Adv. Mater.* **2022**, *34* (36), 2204460.

(15) Lin, K.; Xing, J.; Quan, L. N.; de Arquer, F. P. G.; Gong, X.; Lu, J.; Xie, L.; Zhao, W.; Zhang, D.; Yan, C.; et al. Perovskite Light-Emitting Diodes with External Quantum Efficiency Exceeding 20 per cent. *Nature* **2018**, *562* (7726), 245−248.

(16) Liu, Z.; Qiu, W.; Peng, X.; Sun, G.; Liu, X.; Liu, D.; Li, Z.; He, F.; Shen, C.; Gu, Q.; et al. Perovskite Light-Emitting Diodes with EQE Exceeding 28% through a Synergetic Dual-Additive Strategy for Defect Passivation and Nanostructure Regulation. *Adv. Mater.* **2021**, *33* (43), No. e2103268.

(17) Sun, C.; Jiang, Y.; Cui, M.; Qiao, L.; Wei, J.; Huang, Y.; Zhang, L.; He, T.; Li, S.; Hsu, H.-Y.; et al. High-Performance Large-Area Quasi-2D Perovskite Light-Emitting Diodes. *Nat. Commun.* **2021**, *12* (1), 2207.

(18) Vashishtha, P.; Ng, M.; Shivarudraiah, S. B.; Halpert, J. E. High Efficiency Blue and Green Light-Emitting Diodes Using Ruddlesden-

Popper Inorganic Mixed Halide Perovskites with Butylammonium Interlayers. *Chem. Mater.* **2019**, *31* (1), 83−89.
(19) Ma, J.; Yang, L.; Zhang, Y.; Kuang, Y.; Shao, M. Rearranging the Phase Distribution of Quasi-2D Perovskite for Efficient and Narrow Emission Perovskite Light-Emitting Diodes. *J. Phys. Chem. Lett.* **2022**, *13* (21), 4739−4746.
(20) Li, S.; Luo, J.; Liu, J.; Tang, J. Self-Trapped Excitons in All-Inorganic Halide Perovskites: Fundamentals, Status, and Potential Applications. *J. Phys. Chem. Lett.* **2019**, *10* (8), 1999−2007.
(21) Tan, J.; Li, D.; Zhu, J.; Han, N.; Gong, Y.; Zhang, Y. Self-Trapped Excitons in Soft Semiconductors. *Nanoscale* **2022**, *14* (44), 16394−16414.
(22) Dohner, E. R.; Jaffe, A.; Bradshaw, L. R.; Karunadasa, H. I. Intrinsic White-Light Emission from Layered Hybrid Perovskites. *J. Am. Chem. Soc.* **2014**, *136* (38), 13154−13157.
(23) Smith, M. D.; Jaffe, A.; Dohner, E. R.; Lindenberg, A. M.; Karunadasa, H. I. Structural Origins of Broadband Emission from Layered Pb-Br Hybrid Perovskites. *Chem. Sci.* **2017**, *8* (6), 4497−4504.
(24) Mao, L.; Wu, Y.; Stoumpos, C. C.; Wasielewski, M. R.; Kanatzidis, M. G. White-Light Emission and Structural Distortion in New Corrugated Two-Dimensional Lead Bromide Perovskites. *J. Am. Chem. Soc.* **2017**, *139* (14), 5210−5215.
(25) Thirumal, K.; Chong, W. K.; Xie, W.; Ganguly, R.; Muduli, S. K.; Sherburne, M.; Asta, M.; Mhaisalkar, S.; Sum, T. C.; Soo, H. S.; et al. Morphology-Independent Stable White-Light Emission from Self-Assembled Two-Dimensional Perovskites Driven by Strong Exciton-Phonon Coupling to the Organic Framework. *Chem. Mater.* **2017**, *29* (9), 3947−3953.
(26) Mao, L.; Wu, Y.; Stoumpos, C. C.; Traore, B.; Katan, C.; Even, J.; Wasielewski, M. R.; Kanatzidis, M. G. Tunable White-Light Emission in Single-Cation-Templated Three-Layered 2D Perovskites $(CH_3CH_2NH_3)_4Pb_3Br_{10-x}Cl_x$. *J. Am. Chem. Soc.* **2017**, *139* (34), 11956−11963.
(27) Neogi, I.; Bruno, A.; Bahulayan, D.; Goh, T. W.; Ghosh, B.; Ganguly, R.; Cortecchia, D.; Sum, T. C.; Soci, C.; Mathews, N.; et al. Broadband-Emitting 2D Hybrid Organic-Inorganic Perovskite Based on Cyclohexane-Bis(Methylamonium) Cation. *ChemSusChem* **2017**, *10* (19), 3765−3772.
(28) Cortecchia, D.; Neutzner, S.; Kandada, A. R. S.; Mosconi, E.; Meggiolaro, D.; Angelis, F. D.; Soci, C.; Petrozza, A. Broadband Emission in Two-Dimensional Hybrid Perovskites: The Role of Structural Deformation. *J. Am. Chem. Soc.* **2017**, *139* (1), 39−42.
(29) Smith, M. D.; Connor, B. A.; Karunadasa, H. I. Tuning the Luminescence of Layered Halide Perovskites. *Chem. Rev.* **2019**, *119* (5), 3104−3139.
(30) Chen, J.; Wang, J.; Xu, X.; Li, J.; Song, J.; Lan, S.; Liu, S.; Cai, B.; Han, B.; Precht, J. T.; et al. Efficient and Bright White Light-Emitting Diodes Based on Single-Layer Heterophase Halide Perovskites. *Nat. Photonics* **2021**, *15* (3), 238−244.
(31) Yu, J.; Kong, J.; Hao, W.; Guo, X.; He, H.; Leow, W. R.; Liu, Z.; Cai, P.; Qian, G.; Li, S.; et al. Broadband Extrinsic Self-Trapped Exciton Emission in Sn-Doped 2D Lead-Halide Perovskites. *Adv. Mater.* **2019**, *31* (7), No. e1806385.
(32) Chen, Y.; Wang, Z.; Wei, Y.; Liu, Y.; Hong, M. Exciton Localization for Highly Luminescent Two-Dimensional Tin-Based Hybrid Perovskites through Tin Vacancy Tuning. *Angew. Chem.* **2023**, *62* (18), No. e202301684.
(33) Zhang, J.; Zhu, X.; Wang, M.; Hu, B. Establishing Charge-Transfer Excitons in 2D Perovskite Heterostructures. *Nat. Commun.* **2020**, *11* (1), 2618.
(34) Fang, H.; Tekelenburg, E. K.; Xue, H.; Kahmann, S.; Chen, L.; Adjokatse, S.; Brocks, G.; Tao, S.; Loi, M. A. Unraveling the Broadband Emission in Mixed Tin-Lead Layered Perovskites. *Adv. Opt. Mater.* **2023**, *11* (4), 2202038.
(35) Li, T.; Chen, X.; Wang, X.; Lu, H.; Yan, Y.; Beard, M. C.; Mitzi, D. B. Origin of Broad-Band Emission and Impact of Structural Dimensionality in Tin-Alloyed Ruddlesden-Popper Hybrid Lead Iodide Perovskites. *ACS Energy Lett.* **2020**, *5* (2), 347−352.
(36) Narra, S.; Lin, C.-Y.; Seetharaman, A.; Jokar, E.; Diau, E. W.-G. Femtosecond Exciton and Carrier Relaxation Dynamics of Two-Dimensional (2D) and Quasi-2D Tin Perovskites. *J. Phys. Chem. Lett.* **2021**, *12* (51), 12292−12299.
(37) Seetharaman, A.; Narra, S.; Rajamanickam, P.; Putikam, R.; Lin, M.-C.; Diau, E. W.-G. Diffusion of Bulky Organic Cations in the 3D/2D Heterostructures to Form Interfacial Quasi-2D (N2) Phase for Tin Perovskite Solar Cells. *J. Mater. Chem. A* **2023**, *11* (39), 21089−21098.
(38) Spindler, C.; Galvani, T.; Wirtz, L.; Rey, G.; Siebentritt, S. Excitation-Intensity Dependence of Shallow and Deep-Level Photoluminescence Transitions in Semiconductors. *J. Appl. Phys.* **2019**, *126* (17), 175703.
(39) Simbula, A.; Wu, L.; Pitzalis, F.; Pau, R.; Lai, S.; Liu, F.; Matta, S.; Marongiu, D.; Quochi, F.; Saba, M.; et al. Exciton Dissociation in 2D Layered Metal-Halide Perovskites. *Nat. Commun.* **2023**, *14* (1), 4125.
(40) Wu, X.; Trinh, M. T.; Zhu, X.-Y. Excitonic Many-Body Interactions in Two-Dimensional Lead Iodide Perovskite Quantum Wells. *J. Phys. Chem. C* **2015**, *119* (26), 14714−14721.
(41) Miller, A.; Riblet, P.; Mazilu, M.; White, S.; Holden, T. M.; Cameron, A. R.; Perozzo, P. Exciton Saturation in GaAs Multiple Quantum Wells at Room Temperature. *J. Appl. Phys.* **1999**, *86* (7), 3734−3744.
(42) Rossi, D.; Wang, H.; Dong, Y.; Qiao, T.; Qian, X.; Son, D. H. Light-Induced Activation of Forbidden Exciton Transition in Strongly Confined Perovskite Quantum Dots. *ACS Nano* **2018**, *12* (12), 12436−12443.
(43) Elkins, M. H.; Pensack, R.; Proppe, A. H.; Voznyy, O.; Quan, L. N.; Kelley, S. O.; Sargent, E. H.; Scholes, G. D. Biexciton Resonances Reveal Exciton Localization in Stacked Perovskite Quantum Wells. *J. Phys. Chem. Lett.* **2017**, *8* (16), 3895−3901.
(44) Giovanni, D.; Chong, W. K.; Liu, Y. Y. F.; Dewi, H. A.; Yin, T.; Lekina, Y.; Shen, Z. X.; Mathews, N.; Gan, C. K.; Sum, T. C. Coherent Spin and Quasiparticle Dynamics in Solution-Processed Layered 2D Lead Halide Perovskites. *Adv. Sci.* **2018**, *5* (10), 1800664.
(45) Chen, X.; Lu, H.; Wang, K.; Zhai, Y.; Lunin, V.; Sercel, P. C.; Beard, M. C. Tuning Spin-Polarized Lifetime in Two-Dimensional Metal−Halide Perovskite through Exciton Binding Energy. *J. Am. Chem. Soc.* **2021**, *143* (46), 19438−19445.
(46) Hansen, K. R.; McClure, C. E.; Powell, D.; Hsieh, H.; Flannery, L.; Garden, K.; Miller, E. J.; King, D. J.; Sainio, S.; Nordlund, D.; et al. Low Exciton Binding Energies and Localized Exciton-Polaron States in 2D Tin Halide Perovskites. *Adv. Opt. Mater.* **2022**, *10* (9), 2102698.
(47) Cheng, B.; Li, T.-Y.; Maity, P.; Wei, P.-C.; Nordlund, D.; Ho, K.-T.; Lien, D.-H.; Lin, C.-H.; Liang, R.-Z.; Miao, X.; et al. Extremely Reduced Dielectric Confinement in Two-Dimensional Hybrid Perovskites with Large Polar Organics. *Commun. Phys.* **2018**, *1* (1), 80.

https://doi.org/10.1021/acs.jpcc.3c07717
J. Phys. Chem. C 2024, 128, 1207−1215